British Geological Survey

Expert | Impartial | Innovative

DECOVALEX-2019 project: Task A - modElliNg Gas INjection ExpERiments (ENGINEER)

Minerals and Waste Programme

Open Report OR/18/049

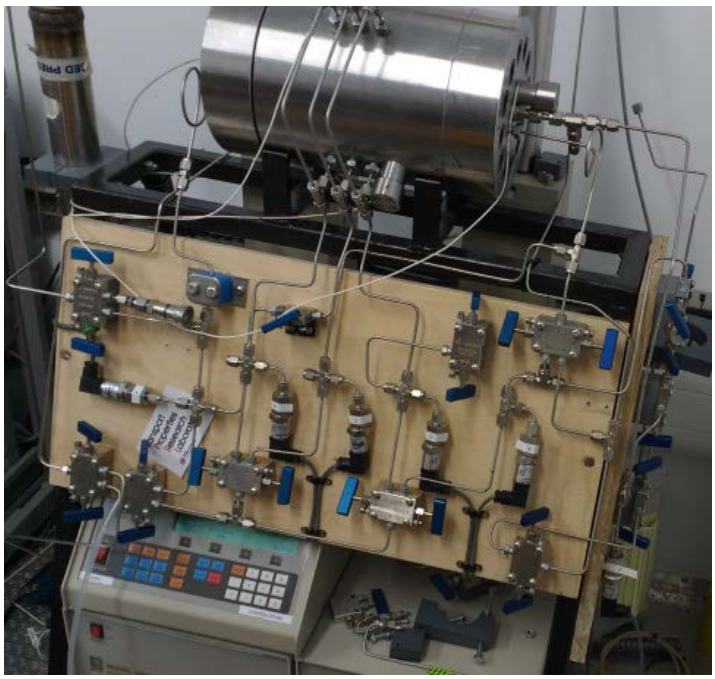

BRITISH GEOLOGICAL SURVEY

MINERALS AND WASTE PROGRAMME

OPEN REPORT OR/18/049

DECOVALEX-2019 project: Task A - modElliNg Gas INjection ExpERiments (ENGINEER)

E. Tamayo-Mas, J.F. Harrington, T. Brüning, O. Kolditz, H. Shao, E.E. Dagher, J. Lee, K. Kim, J. Rutqvist, S.H. Lai, N. Chittenden, Y. Wang, I.P. Damians, S. Olivella

Keywords

Gas flow; Advection; Two-phase flow models; Preferential pathways; Continuous and discrete approaches.

Front cover

Experimental apparatus used for the experiments to be modelled.

Bibliographical reference

TAMAYO-MAS, E., HARRINGTON, J.F., BRÜNING, T., KOLDITZ, O., SHAO, H., DAGHER, E.E., LEE, J., KIM, K., RUTQVIST, J., LAI, S.H., CHITTENDEN, N., WANG, Y., DAMIANS, I.P., OLIVELLA, S.2018. DECOVALEX-2019 project: Task A - modElliNg Gas INjection ExpERiments (ENGINEER). *British Geological Survey Open Report*, OR/18/049. 36pp.

Keyworth, Nottingham British Geological Survey 2018

BRITISH GEOLOGICAL SURVEY

The full range of our publications is available from BGS shops at Nottingham, Edinburgh, London and Cardiff (Welsh publications only) see contact details below or shop online at www.geologyshop.com

The London Information Office also maintains a reference collection of BGS publications, including maps, for consultation.

We publish an annual catalogue of our maps and other publications; this catalogue is available online or from any of the BGS shops.

The British Geological Survey carries out the geological survey of Great Britain and Northern Ireland (the latter as an agency service for the government of Northern Ireland), and of the surrounding continental shelf, as well as basic research projects. It also undertakes programmes of technical aid in geology in developing countries.

The British Geological Survey is a component body of UK Research and Innovation.

British Geological Survey offices

Environmental Science Centre, Keyworth, Nottingham NG12 5GG

Tel 0115 936 3100

BGS Central Enquiries Desk

Tel 0115 936 3143
email enquiries@bgs.ac.uk

BGS Sales

Tel 0115 936 3241
email sales@bgs.ac.uk

The Lyell Centre, Research Avenue South, Edinburgh EH14 4AP

Tel 0131 667 1000
email scotsales@bgs.ac.uk

Natural History Museum, Cromwell Road, London SW7 5BD

Tel 020 7589 4090
Tel 020 7942 5344/45 email bgslondon@bgs.ac.uk

Cardiff University, Main Building, Park Place, Cardiff CF10 3AT

Tel 029 2167 4280

Maclean Building, Crowmarsh Gifford, Wallingford OX10 8BB

Tel 01491 838800

Geological Survey of Northern Ireland, Department of Enterprise, Trade & Investment, Dundonald House, Upper Newtownards Road, Ballymiscaw, Belfast, BT4 3SB

Tel 01232 666595
www.bgs.ac.uk/gsni/

Natural Environment Research Council, Polaris House, North Star Avenue, Swindon SN2 1EU

Tel 01793 411500 Fax 01793 411501
www.nerc.ac.uk

UK Research and Innovation, Polaris House, Swindon SN2 1FL

Tel 01793 444000
www.ukri.org

Website www.bgs.ac.uk
Shop online at www.geologyshop.com

Foreword

This document is the interim report of Task A of the DECOVALEX-2019 project, summarising the outcomes of work in Task A (stages 0 and 1) with work conducted from May 2016 to March 2018. It provides a brief overview of the experimental data, the task structure and a synthesis of the ongoing work of the participating modelling teams as of March 2018.

Acknowledgements

DECOVALEX is an international research project comprising participants from industry, government and academia, focusing on development of understanding, models and codes in complex coupled problems in sub-surface geological and engineering applications; DECOVALEX-2019 is the current phase of the project. The authors appreciate and thank the DECOVALEX-2019 Funding Organisations Andra, BGR/UFZ, CNSC, US DOE, ENSI, JAEA, IRSN, KAERI, NWMO, RWM, SÚRAO, SSM and Taipower for their financial and technical support of the work described in this report. The statements made in the report are, however, solely those of the authors and do not necessarily reflect those of the Funding Organisations. The authors also thank Mrs Fiona McEvoy for her review of the manuscript.

Contents

FIGURES

TABLES

Summary

In a repository for radioactive waste hosted in a clay formation, hydrogen and other gases may be generated due to the corrosion of metallic materials under anoxic conditions, the radioactive decay of waste and the radiolysis of water. If the gas production rate exceeds the gas diffusion rate within the pores of the clay, a discrete gas phase will form and accumulate until its pressure becomes large enough to exceed the entry pressure of the surrounding material.

The purpose of Task A under DECOVALEX-2019 is to better understand the processes governing the advective movement of gas in both low-permeability argillaceous repository host rocks and clay-based engineered barriers. Special attention is given to the mechanisms controlling gas entry, flow and pathway sealing and their impact on the performance of the engineered clay barrier. Previous work suggests gas flow may be accompanied by the creation of dilatant pathways whose properties change temporally and spatially within the medium. Thus, new numerical representations for the quantitative prediction of gas migration fluxes through argillaceous rock formations have been developed. These provide an invaluable tool with which to assess the impact of gas flow on repository layout and therefore design of any future facility. In addition, experience gained through this task is of direct relevance to other clay-based engineering issues where immiscible gas flow is a consideration including shale gas, hydrocarbon migration, carbon capture and storage and landfill design.

Task A is organised into four steps, starting with the code development (stage 0) and followed by the modelling of a 1D gas flow test (stage 1) and a spherical gas flow test (stage 2). Then, the previous models are applied to a natural argillaceous material (stage 3).

This report summarises the outcomes of work in Task A (stages 0 and 1) with work conducted from May 2016 to March 2018 and provides a brief overview of the experimental data, the current task structure and a synthesis of the ongoing work of the participating modelling teams as of March 2018.

1 Introduction

In 1999, Rodwell et al. stated “there are few problems in geoscience more complex than the quantitative prediction of gas migration fluxes through an argillaceous rock formation”. To understand this statement, it is necessary to appreciate why argillaceous materials (which include clays, claystones and mudrocks) differ from other clastic sedimentary rocks. Key factors in this respect include the sub-microscopic dimensions of the interparticle spaces, the very large specific surface of the mineral phases, strong physico-chemical interactions between water molecules and surfaces, very low permeability, generally low tensile strength, a deformable matrix, and a very pronounced coupling between the hydraulic and mechanical response of these materials. It is therefore necessary to consider these properties when defining the behaviour of these materials (both natural and engineered) in order to successfully represent flow in such systems.

With this in mind, the processes governing the movement of repository gases through engineered barriers and clay-rich host rocks can be split into two components, (i) molecular diffusion (governed by Fick’s Law) and (ii) bulk advection. In the case of a repository for radioactive waste, corrosion of metallic materials under anoxic conditions will lead to the formation of hydrogen. Radioactive decay of the waste and the radiolysis of water are additional source terms. If the rate of gas production exceeds the rate of gas diffusion within the pores of the barrier or host rock, a discrete gas phase will form (Wikramaratna et al., 1993; Ortiz et al., 2002; Weetjens and Sillen, 2006). Under these conditions, gas will continue to accumulate until its pressure becomes sufficiently large for it to enter the surrounding material.

In clays and mudrocks, four primary phenomenological models describing gas flow can be defined, Figure 1: (1) gas movement by diffusion and/or solution within interstitial fluids along prevailing hydraulic gradients; (2) gas flow in the original porosity of the fabric, commonly referred to as two-phase flow; (3) gas flow along localised dilatant pathways, which may or may not interact with the continuum stress field; and (4) gas fracturing of the rock similar to that performed during hydrocarbon stimulation exercises.

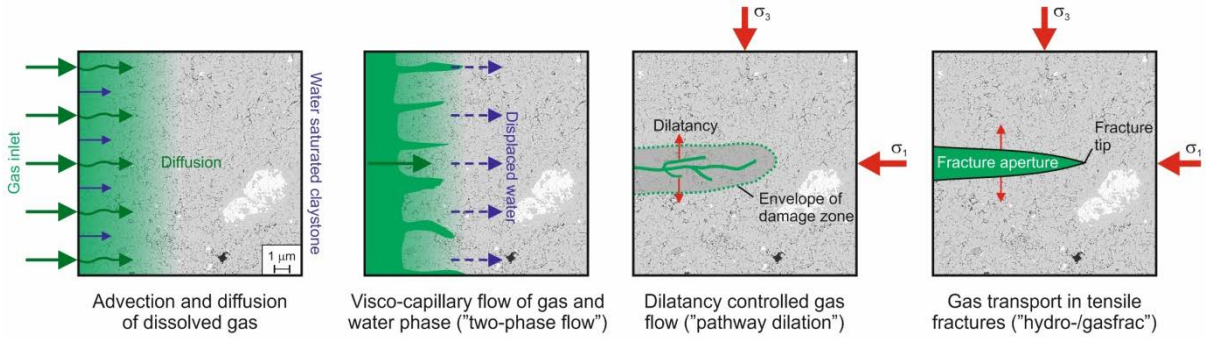

Figure 1 Conceptual models of gas flow (after Marschall et al. 2005), BGS © *UKRI.*

There is now a growing body of evidence (Horseman et al., 1996, 2004; Harrington and Horseman, 1999, 2003; Angeli et al., 2009; Harrington et al., 2017a and b) that in the case of plastic clays and in particular bentonite, classic concepts of porous medium two-phase flow are inappropriate and continuum approaches to modelling gas flow may be questionable, depending on the scale of the processes and resolution of the numerical model. However, the detail of the dilatant mechanisms controlling gas entry, flow and pathway sealing are unclear and the “memory” of such features within clay may impair barrier performance, in particular, acting as preferential flow paths for the movement of radionuclides.

As such, development of new and novel numerical representations for the quantitative treatment of gas in clay-based repository systems are therefore required, and are the primary focus of Task A in the current phase of the DECOVALEX project. New numerical techniques provide an invaluable tool with which to assess the impact of gas flow on repository layout and therefore design of any future facility. In addition, the same processes and mechanisms described in such models are of direct relevance to other clay-based engineering issues where immiscible gas flow is involved e.g. shale gas, hydrocarbon migration, carbon capture and storage and landfill design.

The Task is split into four stages each building on the previous, representing an incremental increase in complexity:

1. Stage 0 (code development): analysis of data, conceptual model and process model development.
2. Stage 1: 1D gas flow
    - 1D gas flow test on saturated bentonite under constant volume (Mx80-D).
3. Stage 2: spherical gas flow
    - A: spherical flow through saturated bentonite under a constant volume boundary condition (Mx80-10).
    - B (optional): spherical flow through saturated bentonite under a constant volume boundary condition (Mx80-A).
4. Stage 3: application to previous models to natural clay-based systems
    - A (optional): triaxial test on Callovo-Oxfordian claystone.
    - B (optional): gas flow in hydrated pellets under constant volume conditions.

This report summarises the outcomes of stages 0 and 1 with work conducted from May 2016 to March 2018 by the participating modelling teams

1. BGR/UFZ (Germany): Federal Institute for Geosciences and Natural Resources and the Helmholtz Centre for Environmental Research.
2. CNSC (Canada): Canadian Nuclear Safety Commission.
3. KAERI (Korea): Korea Atomic Energy Research Institute.
4. LBNL (United States of America): Lawrence Berkeley National Laboratory.
5. NCU/TPC (Taiwan): National Central University and Taiwan Power Company (Taipower).
6. Quintessa/RWM (United Kingdom): Quintessa Ltd on behalf of Radioactive Waste Management.
7. SNL (United States of America): Sandia National Laboratories.
8. UPC/Andra (Spain/France): Universitat Politècnica de Catalunya, funded by l'Agence nationale pour la gestion des des déchets radioactifs.

and presented at the following DECOVALEX workshops:

1. 1st DECOVALEX-2019 Workshop (Berkeley, USA, May 18 – 20, 2016): a general presentation of the task was given (available information and description of the gas flow tests) and a work plan amongst the teams was agreed. Teams were asked to develop one or more modelling approaches to address Stages 1 through 3. A range of approaches were encouraged from highly mechanistic models which may attempt to replicate nearly all aspects of experimental behaviour, to highly simplified homogenised approaches which aim to capture key features of the data.
2. 2nd DECOVALEX-2019 Workshop (Taipei, Taiwan, November 29 - December 1, 2016): first analysis of the 1D gas flow together with any prototype numerical models were presented by the teams. A wide range of modelling approaches were shown.
3. 3rd DECOVALEX-2019 Workshop (Stockholm, Sweden, April 25 – 28, 2017): team approaches were collated and the first key comparison exercise was done. A first attempt

to model the evolution in gas pressure and stress response matching breakthrough times and flux in/out of the core was made.

4. 4th DECOVALEX-2019 Workshop (Kingston, Canada, October 10 – 13, 2017): the different modelling approaches were compared and judged (based on timing, magnitude and shape). Results from that meeting (including work up to March 2018) are reported in this paper.

It is not the intention of this report to provide an exhaustive description of the individual contributions from each team, but rather give a technical overview and synthesis of key conclusions and results.

2 Experimental data

The experiment undertaken by the British Geological Survey (BGS) consisted of a 1D gas injection test performed on a pre-compacted Mx80 bentonite sample supplied by Clay Technology AB (Lund, Sweden), see Table 1 for the sample dimensions and geotechnical parameters and Daniels and Harrington (2017) for a detailed description of the sample preparation and laboratory procedure.

Table 1 Sample dimensions and geotechnical parameters.

Sample	Length [mm]	Diameter [mm]	Weight [g]	Dry density [kg/m^3]	Bulk density [kg/m^3]
Mx80-D	119.88	59.59	671.65	1.56	1.99

As reported by Daniels and Harrington (2017), a constant volume pressure vessel, with a hollow steel cylinder and two detachable end-closures, was used for the testing (see Figure 2 and Harrington and Horseman 2003, for a general description of the employed apparatus). The pressure vessel was instrumented with (i) 2 axial and 3 radial load cells and (ii) 3 radial arrays comprised of 4 spot-filters in each, which allowed the continuous monitoring of pore pressure within each array, see Table 2 for their relative positions. The test comprised two stages; hydration of the sample (Stage 1) followed by gas testing (Stage 2). After gas breakthrough and a period of gas flow through the sample, the injection pump was stopped whilst the swelling pressures (stresses) and pore pressures were continuously monitored.

Table 2 Relative positions of load cells and pore pressure filters.

Array	Sensor name	Axial distance from backpressure face [mm]	Rotation around bore of vessel [degrees]
Axial stress	Injection load cell	120	90
Radial stress	Radial load cell 1	104.8	0
Radial stress	Radial load cell 2	60	120
Radial stress	Radial load cell 3	15.2	240
Axial stress	Backpressure load cell	0	30
Radial pore pressure array 1	Radial 1	81.4	330
	Radial 2	81.4	60
	Radial 3	81.4	150
	Radial 4	81.4	240
Radial pore pressure array2	Radial 5	60	330
	Radial 6	60	60
	Radial 7	60	150
	Radial 8	60	240
Radial pore pressure array 3	Radial 9	38.6	330
	Radial 10	38.6	60
	Radial 11	38.6	150
	Radial 12	38.6	240
Midplane filter	Middle	60	0

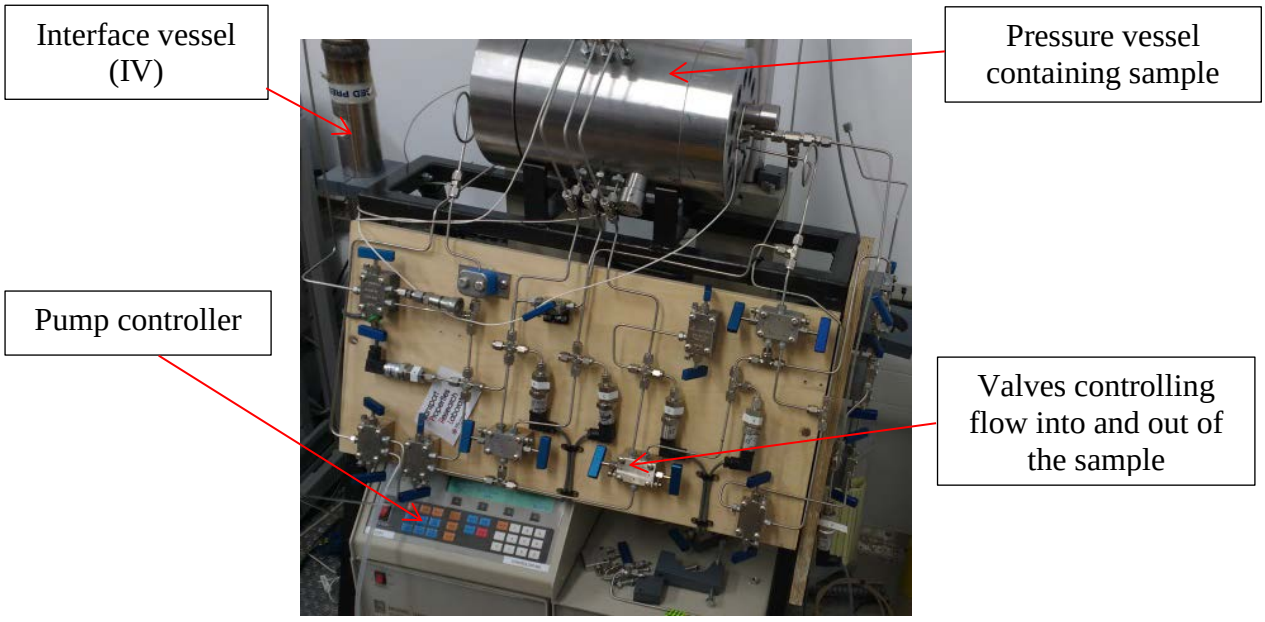

Figure 2 The experimental apparatus and sample assembly.

2.1 SAMPLE HYDRATION

After installation, the sample was allowed to equilibrate with the water in the radial filters and backpressure end-closure filter for a period of 7.3 days, providing sufficient time for the sample to develop enough swelling pressure so that the external pore pressure could be applied. Following this, the sample was allowed to hydrate for a further 32 days until total stress had approached a well-defined asymptote, see monitored stresses and pore pressures for this period in Figure 3 and Figure 4 respectively.

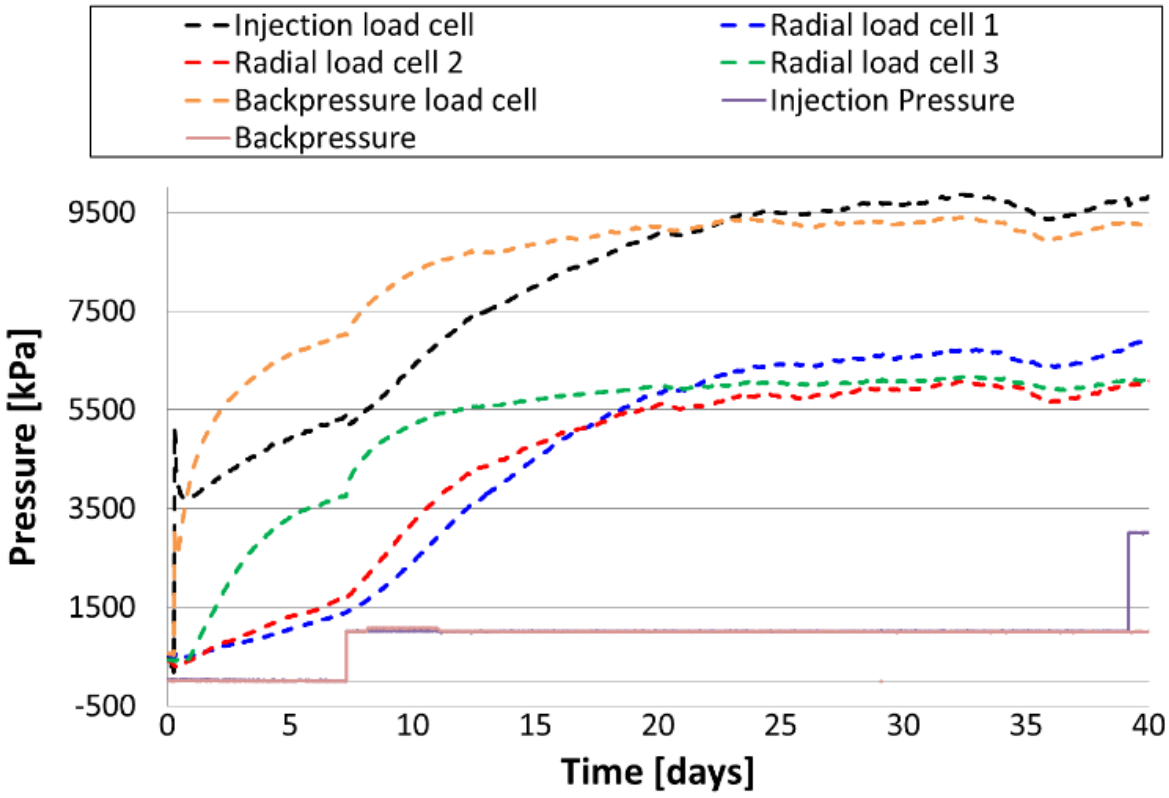

Figure 3 Swelling pressure measured by the axial and radial load cells, injection pressure and backpressure.

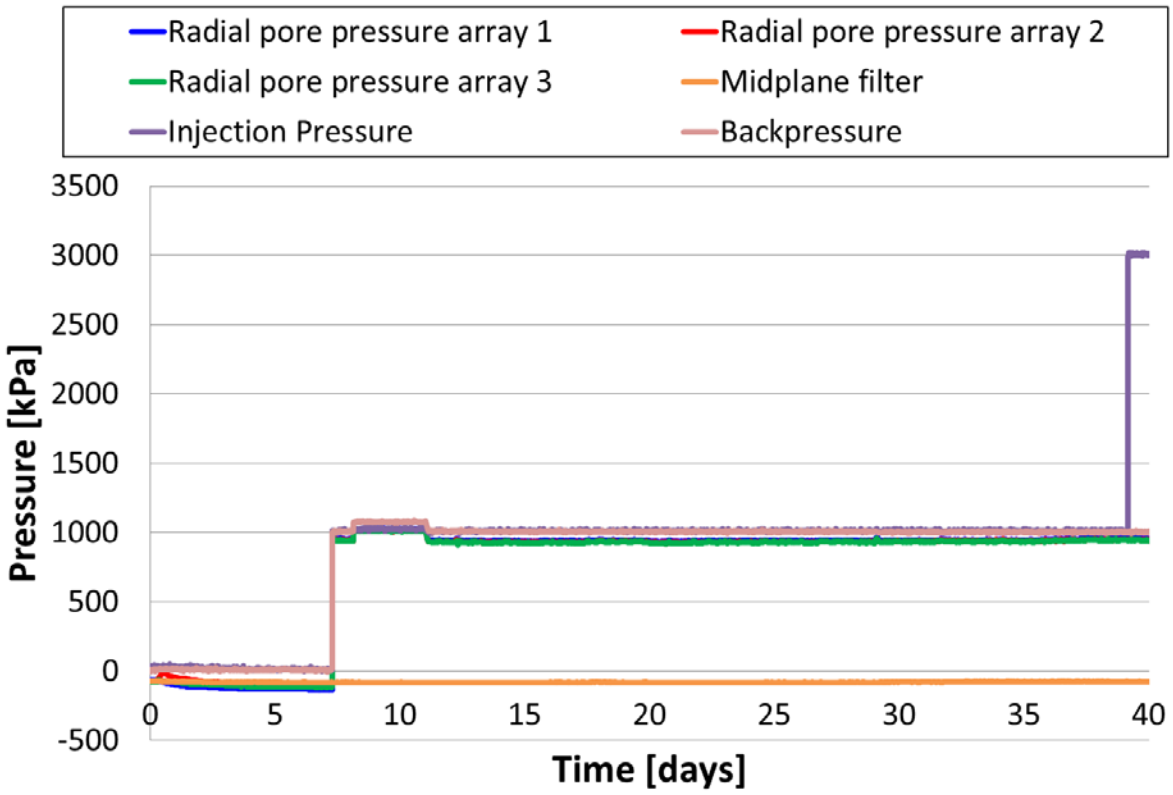

Figure 4 Axial and radial pore pressure for the first 40 days.

2.2 GAS TESTING

Gas testing began on day 39. Additional helium was added to increase gas pressure to 3 MPa. This was then held constant for a period of 7 days to allow the system to equilibrate and to help identify significant leakages. At day 46, the injection pump was then set to a constant flow rate of 500 µl/h and the injection pressure gradually increased for the next 8 days from 3 MPa to 5 MPa whilst the volume of fluid in the injection pump decreased from 102.7 ml to 6.25 ml. At this point (day 54), the fluid in the injection pump was refilled and the flow rate was reduced to 375 µl/h. At day 61 (before the pressure in the injection filter reached the breakthrough pressure), further helium was added to the interface vessel. As such, the injection pump volume increased, see Figure 5 and Figure 6 for the evolution of total stresses and pore pressures.

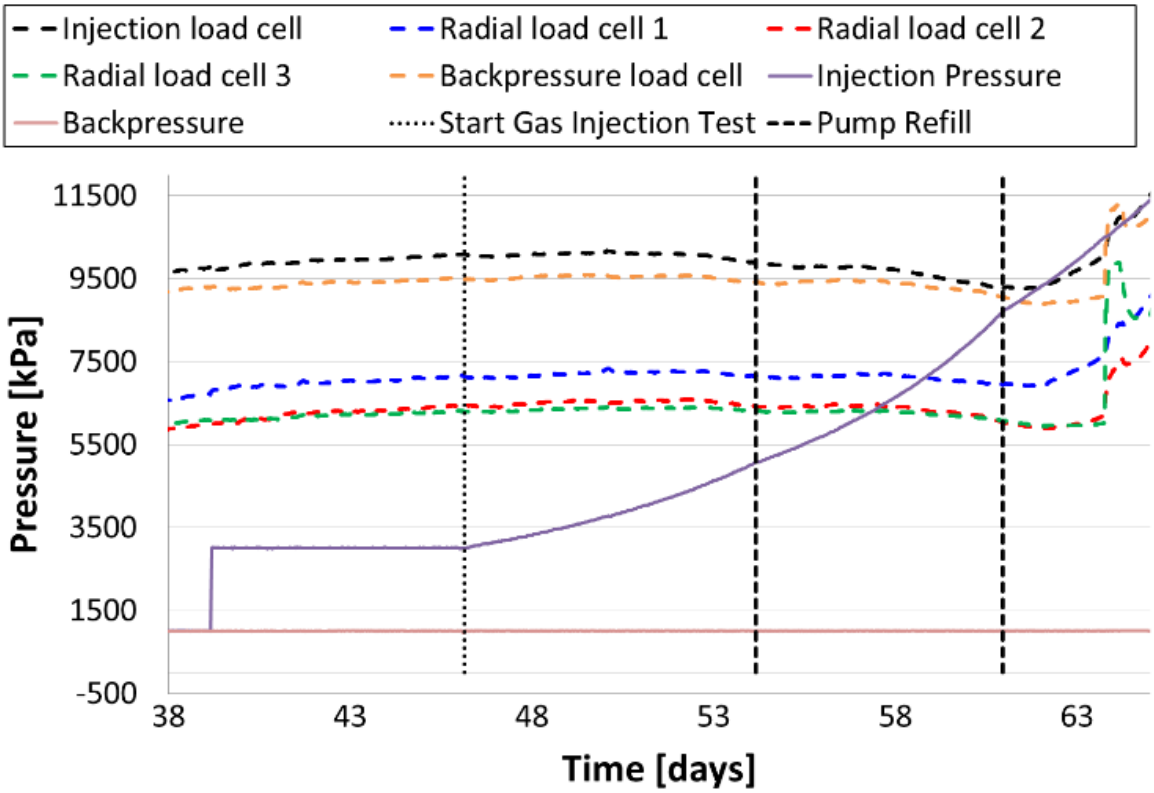

Figure 5 Total stress up to gas breakthrough at 63.5 days.

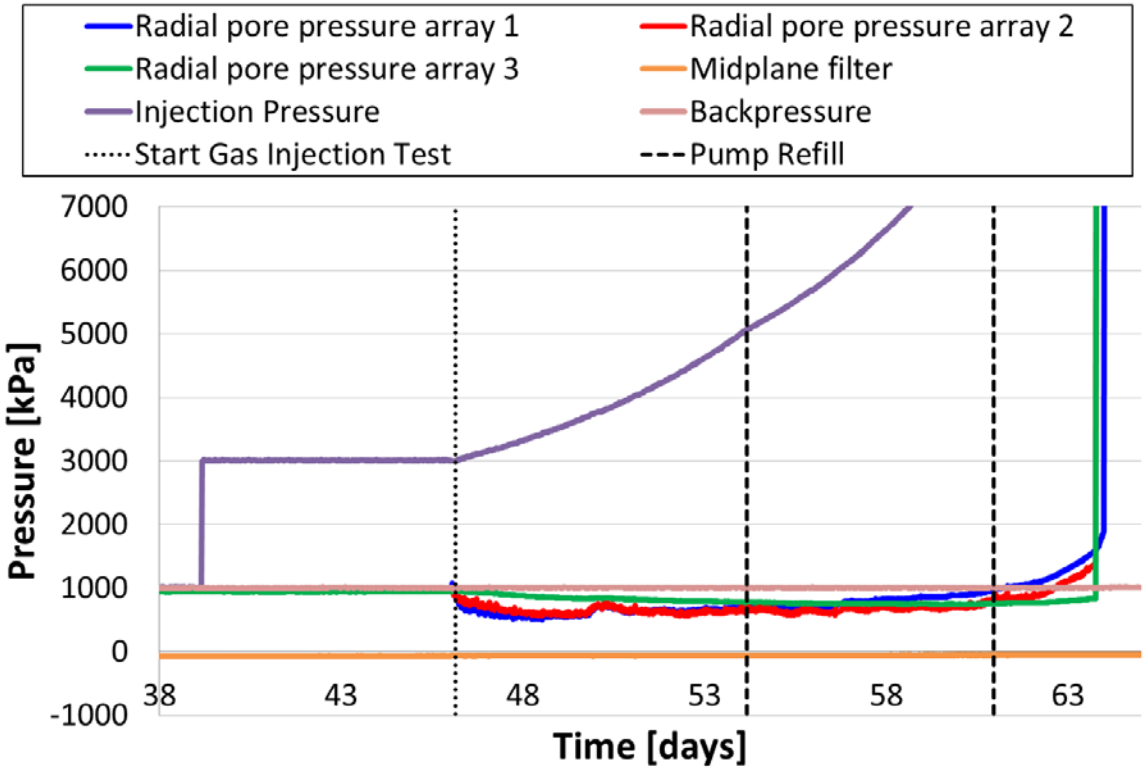

Figure 6 Pore pressures up to gas breakthrough at 63.5 days.

Gas breakthrough occurred at 63.5 days. Interestingly, the increase in pressure in the array closest to the injection face lagged behind those of the other two arrays, suggesting non-uniform gas flow. At day 71, the injection pump was stopped. Between day 71 and day 76, the pore pressures decreased substantially, see Figure 7.

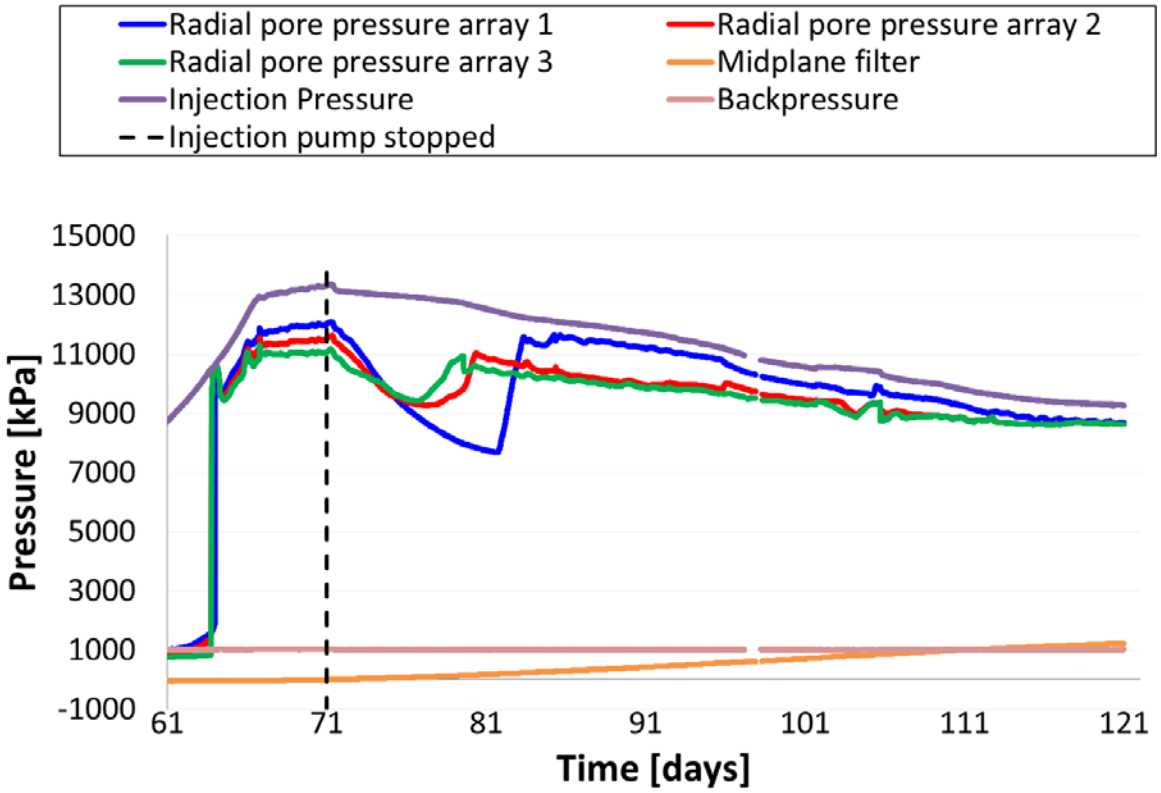

Figure 7 Injection pressure, backpressure and radial pore pressure transducer data from day 61 to day 121.

Examination of the axial and radial load cell data during gas entry and breakthrough, Figure 8, indicates that the swelling pressure (stress) within the sample increased at the same time as gas breakthrough occurred in the backpressure filter. Following gas breakthrough, the system approached a quasi-steady state as gas pressure approached an asymptote and flow in and out of the system began to converge (between days 63.5 and 71). The dip in pore pressure seen in Figure 7 between days 71 and 81 also corresponded with a dip in total stress, and an apparent reduction in outflow. This event appears to occur close to the cessation of pumping. However, by day 81, pore pressures rebounded suggesting the cessation of pumping is not the cause for the spontaneous change in pore pressure.

Following gas breakthrough, total stress and pore pressure appeared integrally linked to the gas pressure within the clay. This is in line with previous observations (Harrington and Horseman, 2003; Harrington et al., 2017a). This continued following the cessation of pumping, as gas pressure and total stress and pore pressure began to decay. During this phase of testing, outflow was sporadic suggesting new gas pathways continued to open and close during this phase of testing. Some of these outflow events correlated with observed changes in total stress and pore pressure, while others did not.

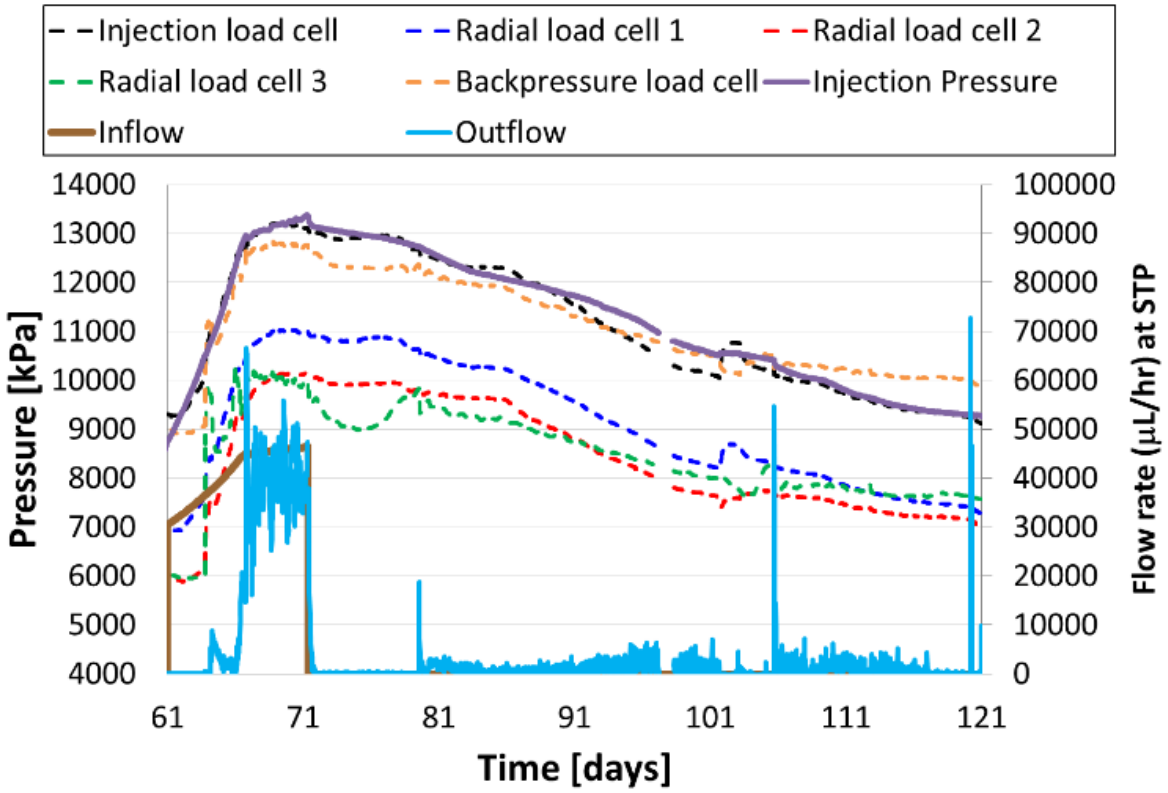

Figure 8 Total stress and flow data from day 61 to day 121.

3 Modelling approaches

Different approaches have been adopted by the participating teams:

1. Classical two-phase flow models, where basic physical principles such as mass and momentum balance apply for each phase. These standard models have been coupled to different mechanical deformation behaviours in order to better represent the experimentally observed flow. In particular, the following deformation models have been considered:
    - Model UPC/Andra-H, with a rigid porous medium (developed by UPC/Andra).
    - Model LBNL-C, where a linear elastic medium is considered (developed by LBNL).
    - Model CNSC-E, where an elastic medium is assumed (developed by CNSC).
    - Model CNSC-D, where a damage medium is assumed (also developed by CNSC).
    - Model KAERI, where a similar damage medium is assumed (developed by KAERI).
    - Model BGR/UFZ, with an elasto-plastic medium (developed by BGR/UFZ).
    - Model NCU/TPC, with a viscoelastic model (developed by NCU/TPC).
2. Enriched two-phase flow models, where preferential pathways are considered:
    - Model Quintessa/RWM: separate gas and water coexist within an elastic deformation matrix (developed by Quintessa/RWM).
    - Model UPC/Andra-HM1: embedded fracture permeability model where deformation is modelled assuming elasticity with effective stress and suction terms (developed by UPC/Andra).
    - Model UPC/Andra-HM2: embedded fracture permeability model where deformation is modelled assuming elasticity with effective stress and without suction terms (developed by UPC/Andra).

3. Discrete approaches, where fractures are explicitly modelled:
    - Model LBNL-D: a two-phase flow model within a discrete fracture network (developed by LBNL).
    - Model SNL: a conceptual chaotic model developed by SNL.

Differences between the proposed strategies also lie in the software used by the teams (Table 3) and in the assumed geometry to represent the saturated bentonite (Table 4).

Table 3 Codes used by the participating teams.

Model	Software	Reference
BGR/UFZ	OpenGeoSys	Kolditz et al., 2012
CNSC-E	COMSOL Multiphysics®	COMSOL, 2017
CNSC-D		
KAERI	TOUGH-MP FLAC3D	Zhang et al., 2008, Itasca 2018
LBNL-C	TOUGH-FLAC	Rutqvist, 2011
LBNL-D	TOUGH-RBSN	Asahina et al., 2014
NCU/TPC	THMC 7.1	Yeh et al., 2013
Quintessa/RWM	QPAC	Quintessa, 2013
UPC/Andra-H	CODE_BRIGHT	Olivella et al., 1996
UPC/Andra-HM1		
UPC/Andra-HM2		

Table 4 Test geometries used by the teams.

Model	Geometry	Mesh	Discretisation
BGR/UFZ	2D axisymmetric	Triangle	2715 elements 1447 nodes
CNSC-E	3D	Tetrahedral	22000 elements
CNSC-D	3D	Tetrahedral	22000 elements
KAERI	3D	Hexahedral	7560 elements 8450 nodes
LBNL-C	3D	Hexahedral	23400 elements 24939 nodes
LBNL-D	2D	Cells and lattice	1401 cells 3840 lattice elements
NCU/TPC	2D	Quadrilateral	1250 elements 1326 nodes
Quintessa/RWM	1D finite volume	-	20 cells +1 abstract cell to simulate mass balance in the injector
UPC/Andra-H	3D	Hexahedral	7168 elements 7917 nodes
UPC/Andra-HM1			
UPC/Andra-HM2			

In order to calibrate and validate these strategies, teams used different parameters and calibration techniques. As seen in Table 5, almost all the teams used for their simulations the following given basic parameters:

1. Young's modulus: $E = 307$ MPa.
2. Poisson's ratio: $\nu = 0.4$.
3. Porosity: $\phi = 0.44$.
4. Intrinsic permeability: $k = 3.4 \times 10^{-21}$ m^2.

However, in order to improve their calibrated results, some teams (BGR/UFZ, NCU/TPC, UPC/Andra) have used a Young's modulus and initial permeability and porosity values significantly different from those of the material. Another difference amongst the proposed strategies is the amount of parameters that need to be calibrated to fit experimental results. As seen in Table 6, the complexity of the physical process requires a detailed (and sometimes cumbersome) calibration process.

Table 5 Basic fixed parameters used by the teams.

Model	Basic fixed parameters			
	E [MPa]	**ν [-]**	**ϕ [-]**	**k [m^2]**
BGR/UFZ	307	0.4	0.44	calibrated
CNSC-E	307	0.4	0.44	3.4×10^{-21}
CNSC-D	307	0.4	0.44	3.4×10^{-21}
KAERI	307	0.4	0.44	3.4×10^{-21}
LBNL-C	307	0.4	0.44	3.4×10^{-21}
LBNL-D	307	0.4	Heterogeneous ($\phi_0 = 0.44$)	3.4×10^{-21}
NCU/TPC	307	0.4	0.43	calibrated
Quintessa/RWM	307	0.4	-	3.4×10^{-21}
UPC/Andra-H	-	-	Heterogeneous ($\phi_0 = 0.36$-0.38)	calibrated
UPC/Andra-HM1	225	0.125	Heterogeneous ($\phi_0 = 0.36$-0.38)	calibrated
UPC/Andra-HM2	307	0.44	0.41	calibrated

Table 6 Calibrated parameters used by the teams.

Model	Calibrated parameters
BGR/UFZ	Intrinsic permeability: 1×10^{-21} m^2 Critical pressure
CNSC-E	Air-entry value
CNSC-D	Air-entry value Minimum air-entry value Maximum intrinsic permeability Damage smoothing parameter Swelling coefficient
KAERI	Damage parameters: tensile strength, residual tensile strength, tensile strain limit, maximum damage value, maximum permeability
LBNL-C	Hydro-mechanical coupling parameters: swelling coefficient, maximum aperture for stress, reference stress Effective gas-entry pressure value

LBNL-D	Mohr-Coulomb failure parameters Effective gas-entry pressure value Swelling coefficient
NCU/TPC	Intrinsic permeability: 3.4×10^{-22} m^2 Air-entry value Viscous parameters
Quintessa/RWM	Capillarity compressibility Capillary spacing Swelling pressure Biot coefficient
UPC/Andra-H	Intrinsic permeability: Het. $k_0 = 5.59 \times 10^{-18}$ m^2
UPC/Andra-HM1	Intrinsic permeability: Het. $k_0 = (2.15 - 7.10) \times 10^{-18}$ m^2 Embedded permeability parameters
UPC/Andra-HM2	Intrinsic permeability: Het. $k_0 = (2.15 - 7.10) \times 10^{-19}$ m^2 Embedded permeability parameters

3.1 CLASSICAL TWO-PHASE FLOW MODELS

Different approaches have been proposed. All of them assume the standard van Genuchten (1980) model to describe the water retention curve but they differ in the assumed mechanical deformation behaviour.

3.1.1 Model UPC/Andra-H

UPC/Andra developed a two-phase flow calculation on a 3D rigid medium (model UPC/Andra-H). In this model, porosity ϕ [-] is assumed to be space-dependent and it is heterogeneously distributed (randomly generated in the range of 0.36 – 0.38). The intrinsic permeability k [m^2] is porosity-dependent and it is given by the exponential function

$$k = k_0 e^{b_k(\phi - \phi_0)} \tag{1}$$

where k_0, ϕ_0 and b_k are equation definition parameters. Here the calibrated values $k_0 = 5.59 \times 10^{-18}$ m^2 and $b_k = 60$ have been used. The retention curve is also porosity-dependent and it is computed as

$$S = \left(1 + \left(\frac{p_g - p_l}{p_{vG}}\right)^{\frac{1}{1-\lambda_{vG}}}\right)^{-\lambda_{vG}} \tag{2}$$

where both the gas pressure p_g [Pa] and the water pressure p_l [Pa] are computed according to the van Genuchten model, λ_{vG} is the shape function and p_{vG} [Pa] is the capillary pressure

$$p_{vG} = p_{vG}^0 e^{b_{vG}(\phi_0 - \phi)} \tag{3}$$

with p_{vG}^0 [Pa] and b_{vG} two extra equation parameters. In this model, $\lambda_{vG} = 0.45$, $p_{vG}^0 = 27$ MPa and $b_{vG} = 33$.

3.1.2 Model LBNL-C

In the poro-elastic model LBNL-C, the effective stress is expressed as

$$\boldsymbol{\sigma}' = \boldsymbol{\sigma} - p^{\phi}\mathbf{I} \tag{4}$$

where $\boldsymbol{\sigma}'$ and $\boldsymbol{\sigma}$ are the effective and total stress tensors respectively, $\mathbf{I}$ is the identity tensor and the pore pressure p^{ϕ} is defined as

$$p^{\phi} = \max(p_l, p_g) \tag{5}$$

with p_l and p_g liquid and gas phase pressures respectively.

This model assumes that the bentonite behaves elastically, with a volumetric swelling and a swelling stress that depends on the changes in water saturation ΔS_l, according to

$$\Delta \boldsymbol{\sigma}'_{\mathrm{sw}} = \mathbf{K} \Delta S_l \beta_{\mathrm{sw}} \tag{6}$$

where $\boldsymbol{\sigma}'_{\mathrm{sw}}$ [Pa] is the swelling stress, **K** [Pa] is the bulk modulus, S_l [-] is the liquid saturation and β_{sw} [-] is a calibrated moisture swelling coefficient ($\beta_{\mathrm{sw}} = 0.02$).

This model assumes a fracture-like behaviour of the flow path. Hence, a pressure dependent permeability function

$$k = k_{\mathrm{matrix}} + \frac{b_h^3}{12a} \tag{7}$$

is considered, where a [m] is the element width and b_h [m] is a non-linear function of the effective minimum compressive stress that reads

$$b_h = \frac{b_{h0}}{1 + 9\left(\frac{\sigma_n - P}{\sigma_{n,\,\mathrm{ref}}}\right)} \tag{8}$$

with b_{h0} [m] being the (calibrated) maximum aperture for permeability (b_{h0}=2.9 μm), σ_n [Pa] the total stress normal to the fracture and $\sigma_{n,\,\mathrm{ref}}$ [Pa] the adjusted reference stress normal to the fracture ($\sigma_{n,\,\mathrm{ref}}$ =0.2 MPa). The aperture versus pressure relationship of Eq. (8) corresponds to the Bandis et al. (1983) model and its parameters are calibrated by matching pressure and outflow responses observed in the experiments.

3.1.3 Model CNSC-E

The three-dimensional model CNSC-E proposed by CNSC assumes an elastic deformation of the solid material. In this model, the presence of the pore gas phase is accounted by defining the average pore fluid pressure

$$p = (1 - \chi) p_g + \chi p_l \tag{9}$$

where χ [-] is a function of the matric suction s [Pa] and the air entry suction s_e [Pa] (here calibrated to s_e =9.81 MPa) determined from the Khalili and Khabbaz (1998) equation

$$\chi = \begin{cases} 1, & \text{if } s \le s_e \\ \left(\frac{s}{s_e}\right)^{-0.55}, & \text{if } s > s_e \end{cases} \tag{10}$$

3.1.4 Model CNSC-D

An enhanced version of the above-mentioned model is the damaged-based model CNSC-D, also proposed by CNSC. Model CNSC-D assumes a continuum elastic-damage bulk (Fall et al., 2014), where the rock may progressively degrade due to microcracks. Thus, according to continuum elastic-damage mechanics, the stiffness of the material depends on a damage parameter D ($0 \le D \le 1$) and reads

$$E = E_0(1 - D^c) \tag{11}$$

where E_0 [Pa] is the initial stiffness and c [-] (c = 10) is the calibrated damage smoothing parameter (note that both the rock and its damage are assumed isotropic and elastic and thus, E, E_0 and D are all scalar). The intrinsic permeability of this model is also damage dependent and it is computed by means of

$$k = k_{\mathrm{undam.}} + k_{\mathrm{dam.}}(D) \tag{12}$$

where

$$k_{\text{dam.}} = D^c(k_{\max} - k_{\text{undam.}}) \quad (13)$$

with $k_{\max}$ [m^2] being a calibrated maximum intrinsic permeability ($k_{\max} = 1.00 \times 10^{-18}$ m^2). In this model, the swelling induced volume change dε_{vs} is related to the change in suction ds by the equation

$$\mathrm{d}\varepsilon_{\text{vs}} = -B_s \mathrm{ds} \quad (14)$$

where B_s [Pa-1] is a calibrated swelling coefficient, Nasir et al. (2016).

3.1.5 Model KAERI

Another damage-based model was proposed by KAERI. Again, bentonite degradation due to microcracks is taken into account by means of the tensile/compressive damage model proposed by Fall et al. (2014). That is, damage variable under tension is described as

$$D = \begin{cases} 0, & \text{if } \varepsilon_{t0} \le \varepsilon \\ 1 - \dfrac{f_{\text{tr}}}{E_0 \varepsilon}, & \text{if } \varepsilon_{tu} \le \varepsilon \le \varepsilon_{t0} \\ 1, & \text{if } \varepsilon \le \varepsilon_{tu} \end{cases} \quad (15)$$

where f_{tr} [Pa] is the calibrated residual tensile strength (f_{tr} = 0.2 MPa) and ε_{t0} [-] and ε_{tu} [-] are the initial and final tensile strain thresholds respectively (ε_{tu}=5 × 10^{-3}). At the same time, damage variable under compression reads

$$D = \begin{cases} 0, & \text{if } \varepsilon < \varepsilon_{\text{co}} \\ 1 - \dfrac{f_{\text{cr}}}{E_0 \varepsilon}, & \text{if } \varepsilon_{\text{co}} \le \varepsilon \end{cases} \quad (16)$$

where f_{cr} [Pa] is the residual compressive strength (f_{cr} = 3 MPa) and ε_{co} [-] is the compressive threshold strain. The intrinsic permeability of this model is also characterised by Eq. (12) and (13). In this case, the calibrated maximum intrinsic permeability is assumed to be one order of magnitude smaller than in model CNSC-D ($k_{\max} = 1.00 \times 10^{-19}$ m^2).

3.1.6 Model BGR/UFZ

In model BGR/UFZ, a critical pressure p_{crit} [Pa] is introduced and calibrated, which is a sum of the minimal principal stress (confining pressure) and the gas entry pressure. The dilatancy pathway is expressed by permeability change (Xu et al., 2013)

$$k = \begin{cases} (1 + 0.0125 p_g) k_{\text{int}}, & p_g \le p_{\text{crit}} \\ (15.2 p_g - 485) k_{\text{int}}, & p_g > p_{\text{crit}} \end{cases} \quad (17)$$

3.1.7 Model NCU/TPC

In model NCU/TPC, a viscoelastic deformation behaviour is assumed. In this model, intrinsic permeability is a non-linear function of porosity and reads

$$k = k_0 \left(\frac{1}{1 + (\phi_0 - \phi)} \right)^n \quad (18)$$

where k_0 [m^2] and ϕ_0 [-] are the reference intrinsic permeability and the reference porosity respectively and n is the fractional exponent depending on the particle size and packing structure. Note that at this moment in time, see Section 4, this model is not able to correctly reflect the physics of the experiment and further development is needed.

3.2 ENRICHED TWO-PHASE FLOW MODELS WITH PREFERENTIAL PATHWAYS

Three different enriched two-phase flow continuum models have been considered. In these approaches, the bentonite matrix behaves as a linear elastic medium, where preferential gas pathways are included.

3.2.1 Model Quintessa/RWM

Quintessa/RWM developed a model with separate gas and water pathways. The model considers the saturated bentonite as two components: (i) the clay solid "grains" with the non-mobile interlayer water and (ii) the "free" water component. Darcy's law is assumed to describe the "free" water movement with water permeability k_w [m^2]

$$k_w = k_{\text{int}} \tag{19}$$

whereas gas movement is modelled through the Hagen-Poiseuille law. Thus, the opening (and closure) of gas pathways is represented through the capillary radius and its relationship to gas permeability k_g [m^2]

$$k_g = \frac{\pi r^4}{8a} \tag{20}$$

where a [m^2] is the calibrated capillary spacing (a = 5.66× 10^{-6} m^2). The capillary radius r [m] is considered to be dependent on the capillarity compressibility γ [m^{2}Pa^{-1}] (assumed to be γ = 1× 10^{-20} m^{2}Pa^{-1}) through

$$r = r_0 + \frac{\gamma}{r_0}(\epsilon_c(p_g) - \epsilon_{c0}) \tag{21}$$

where r_0 [m] is the reference capillary radius (r_0 = 0.05 μm), ϵ_c [Pa] is the stress for the capillary compressibility, ϵ_{c0} [Pa] is the reference stress for the capillary compressibility (ϵ_{c0} = 0 MPa) and p_g [Pa] is the gas pressure. As seen by means of Eq. (20) and (21), the coupling of the stresses to the permeability is done through the capillarity radius. In order to model the ceasing of gas flow observed in Figure 8, Quintessa/RWM proposed a simple model of the gas injection system based on the ideal gas law.

3.2.2 Model UPC/Andra-HM1

UPC/Andra-HM1 is the first hydro-mechanical model developed by UPC/Andra. This model is based on the embedded fracture model proposed by Olivella and Alonso, 2008. The basic idea of this model consists in properly representing single fractures embedded in a continuous matrix. These fractures are characterized by their aperture b [m] and spacing a [m] thus leading to an intrinsic permeability

$$k = k^{\text{mat}} + k^{\text{frac}} = \frac{k_0(1-\phi_0)^2}{\phi_0^3}\frac{\phi^3}{(1-\phi)^2} + \frac{b^3}{12a} \tag{22}$$

where ϕ_0 [-] is the initial porosity, k_0 [m^2] is the reference permeability and ϕ [-] is the porosity. As done with the hydraulic model UPC/Andra-H, porosity is assumed to be space-dependent and it is heterogeneously distributed (randomly generated with ϕ_0 taking values 0.36, 0.37 and 0.38 with a weight of 1/3 each). In this first model, initial intrinsic permeability is also heterogeneous: a random initial intrinsic permeability with k_0 taking values 2.15× 10^{-18} m^2, 3.90× 10^{-18} m^2 and 7.10× 10^{-18} m^2 with a weight of 1/3 each is considered. This model assumes the same relative permeability for both matrix and fractures. Hence, gas permeability reads

$$k_g = k_{rg}\, k = k_{rg}\left(\frac{k_0(1-\phi_0)^2}{\phi_0^3}\frac{\phi^3}{(1-\phi)^2} + \frac{b^3}{12a}\right) \tag{23}$$

where Eq. (22) has been used.

3.2.3 Model UPC/Andra-HM2

An enhanced version of the previous hydro-mechanical model is also proposed by UPC/Andra. In this second hydro-mechanical model (the so-called UPC/Andra-HM2), different relative permeabilities for the matrix and fractures are assumed. Hence, gas permeability reads

$$k = k_{rg}^{\text{mat}} \frac{k_0(1-\phi_0)^2}{\phi_0^3} \frac{\phi^3}{(1-\phi)^2} + k_{rg}^{\text{frac}} \frac{b^3}{12a} \tag{24}$$

In this second model, a higher fixed initial porosity (ϕ_0= 0.41) is assumed whereas initial intrinsic permeability is one order of magnitude smaller than in model UPC/Andra-HM1: indeed, k_0 is also heterogeneous and randomly generated with values 2.15× 10^{-19} m^2 (weight 1/6), 3.90× 10^{-19} m^2 (weight 1/6) and 7.10× 10^{-19} m^2 (weight 2/3).

3.3 DISCRETE APPROACHES

3.3.1 Model LBNL-D

LBNL proposed a discrete technique where a two-phase flow model is coupled to a discrete fracture network (DFN). In particular, the rigid-body-spring network (RBSN) approach, which can be categorized as a lattice model and is based on the rigid-body-spring model developed by Kawai (1978), is assumed to characterize the mechanical and fracture-damage behavior. Thus, the fracture process of a local rigid-body-spring element is realized by degrading the springs. Hence, the stiffness matrix reads

$$\boldsymbol{E} = (1-D)\boldsymbol{E} \tag{25}$$

where, similarly as the proposed damage strategies (see Eq. (11)), D is a scalar parameter ($0 \leq D \leq 1$). In LBNL-D model, D is directly switched from 0 to 1 once a fracture event occurs, i.e. once the stress state of an element violates the Mohr-Coulomb criteria. As done by UPC/Andra, see Eq. (22), the permeability is porosity-dependent and reads

$$k = \begin{cases} \dfrac{k_0(1-\phi_0)^2}{\phi_0^3} \dfrac{\phi^3}{(1-\phi)^2}, & \text{if unfractured} \\ k_0 + \dfrac{b^3}{12a}, & \text{if fractured} \end{cases} \tag{26}$$

where again, ϕ_0 [-] is the initial porosity, k_0 [m^2] is the reference permeability, ϕ [-] is the porosity, b [m] is the fracture aperture and a [m] is the element width. In this model, as done by CNSC with model CNSC-D, a swelling effect is considered. Here, swelling induced volume change $d\varepsilon_{vs}$ is related to the change in liquid saturation dS by the equation

$$d\varepsilon_{vs} = \alpha_s dS \tag{27}$$

where α_s [-] is the swelling coefficient which is calibrated to match the peak values of total stress responses (α_s = 0.1).

3.3.2 Model SNL

Another conceptual model, where special emphasis is placed on the capture of dilatancy was proposed by SNL. This is based on the concept of the delay logistic model (Strogatz, 2001; Bani-Yaghoub, 2017). The model underlying assumption is that given the low permeability of the material, the dominant mechanism for gas migration is first to form a bubble nucleation and then to push the bubble through the clay matrix through matrix dilation and fracturing. Thus, the evolution of mass and pressure within a bubble of a volume V is simply expressed by

$$\frac{dM}{dt} = k_u(P_u - P) - k_d(P - P_d) \quad (28)$$

where M is the gas mass in the bubble; P is the gas pressure in the bubble; P_u and P_d are the gas pressures in the upstream and the downstream of the bubble movement respectively; k_u and k_d are the permeability of the matrix in the upstream and the downstream of the bubble movement respectively; and t is the time.

For the sake of simplicity, k_u and k_d are assumed to be proportional to the gas pressure P. Thus,

$$k_u = k_u^0 P \quad (29)$$

$$k_d = k_d^0 P \quad (30)$$

where k_u^0 and k_d^0 are constant. Then, and assuming the ideal gas law, Eq. (28) becomes the continuous logistic equation

$$\frac{dP}{dt} = \lambda_1 P\left(1 - \frac{P}{K}\right) \quad (31)$$

with

$$\lambda_1 := \frac{(k_u^0 P_u + k_d^0 P_d)RT}{V} \quad (32)$$

$$K := \frac{\lambda_1}{\lambda_2} \quad (33)$$

$$\lambda_2 := \frac{(k_u^0 + k_d^0)RT}{V} \quad (34)$$

In order to account for the clay "memory" effect, the permeabilities k_u and k_d are assumed to depend not only on the current pressure value (see Eq. (29) and (30)) but on the pressure history. Thus, Eq. (31) becomes

$$\frac{dP}{dt} = \lambda_1\left(1 - \frac{P}{K}\right)\int_{-\infty}^{t} G(t-s)p(s)\mathrm{d}s \quad (35)$$

where $G(t)$ is a kernel function.

Due to the preliminary nature of this novel technique, this is not taken into account in the comparison analysis of Section 4.

4 Results

Inflow results were analysed by the teams. However, some modelling teams fitted the inflow into the injection system whereas some other teams calibrated their strategies by means of the inflow into the sample. Thus, the analysis of the inflow modelling results does not provide meaningful information and therefore has not been included in this report.

Figure 9 shows the outflow results, see Table 7 for a summary. Model BGR/UFZ is not able to correctly capture the shape of the post-breakthrough curve (there is some delay with respect to the observed data) but similar peak values are obtained. Similar comments apply to LBNL-C and LBNL-D models; although the peak outflow value is reasonably well captured, the overall shape of the modelled outflow curve is not well described. The two models proposed by CNSC (both CNSC-E and CNSC-D) fail in describing the outflow data and the results are four orders of magnitude smaller than the experimentally observed; whereas the damaged-based KAERI model reasonably describes the shape of the experimentally-observed outflow. The three approaches presented by UPC/Andra fail in fitting this curve. Indeed, although the calculated outflow is slightly better fitted by the hydraulic model (UPC/Andra-H) than by the hydro-mechanical models, the peak value in this case is only about 40% of the observed values. On the contrary, model

Quintessa/RWM leads to a good representation of the value at the breakthrough. However, the shape of the simulated curve is not properly captured.

Table 7 Capabilities of the proposed models regarding flow.

Model	Outflow	
	Peak value	Post-peak shape
BGR/UFZ	✓	
CNSC-E		
CNSC-D		
KAERI		✓
LBNL-C	✓	
LBNL-D	✓	
NCU/TPC	-	
Quintessa/RWM	✓	
UPC/Andra-H		
UPC/Andra-HM1		
UPC/Andra-HM2		

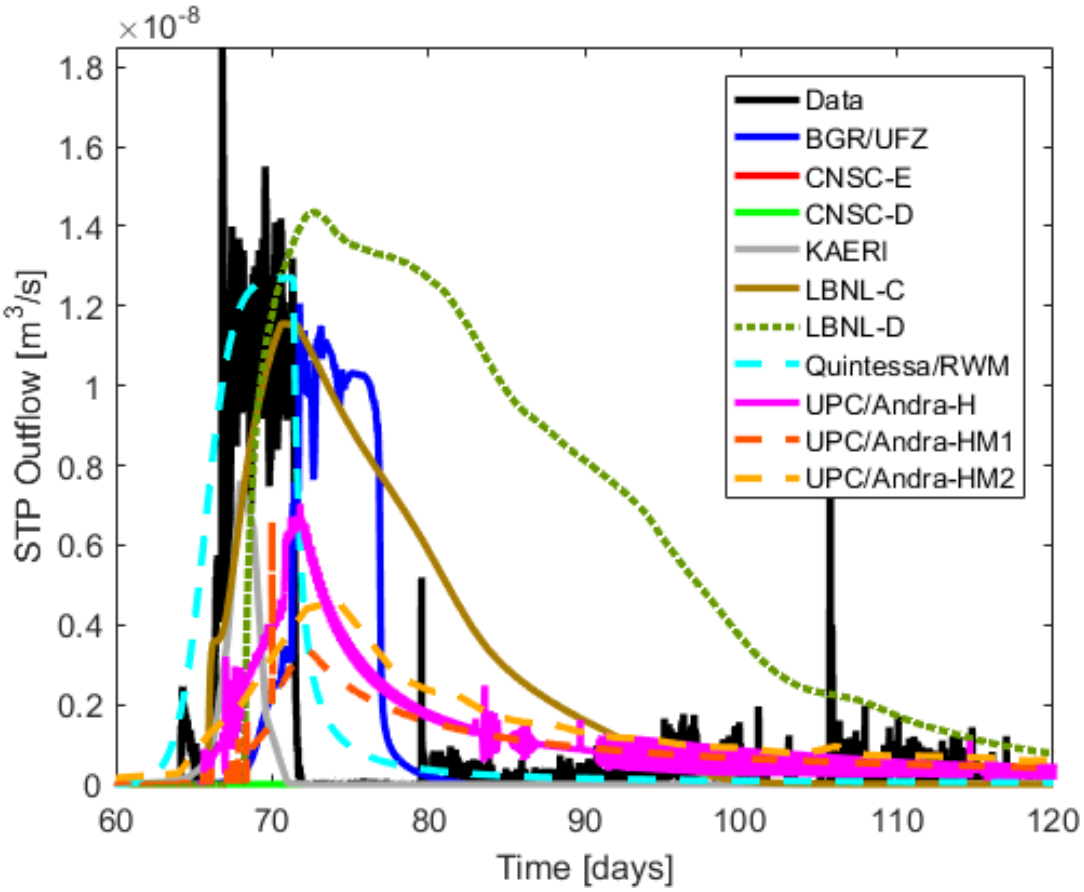

Figure 9 Comparison of modelled versus observed outflow results.

Stress results are shown in Figure 10. As seen, evolution of stress at five different locations has been studied (at the injection load cell, at the backpressure load cell and at three different radial load cells). Although the description of the stress response during the hydration phase (from 0 to 39 days) is a key aspect, little effort was spent by the teams fitting this first stage. As observed, the models Quintessa/RWM and LBNL-C are the only models that properly capture the peak stress value at all the monitored sensors. Model BGR/UFZ is able to correctly capture this value along radial load sensors 1, 2 and 3. However, its prediction of the peak stress value at the backpressure load cell slightly underpredicts the measured value (it should be noted that BGR/UFZ did not postprocess the stress at the injection load cell and thus, BGR/UFZ model cannot be assessed in this point). At the radial load cells 1, 2 and 3, the peak stress value obtained by the rest of the modelling participants either underpredicts the physically-observed quantity (see CNSC-E) or overpredicts it (see damaged-based KAERI model, the hydro-mechanical models by UPC/Andra and the discrete model LBNL-D). CNSC-D is able to capture the peak value at load cell 1 but underpredicted values are obtained at load cells 2 and 3. The predicted value at the injection load cell obtained by UPC/Andra, KAERI and LBNL-D is well defined whereas at the backpressure load cell is underpredicted (UPC/Andra, KAERI) or overpredicted (LBNL-D). The post-peak shape trend is well defined by almost all models and only Quintessa/RWM, CNSC-E and LBNL-C fail in describing the post-peak curve. A visual inspection of the data indicates that many of the teams are able to capture the rapid increase in stress at similar times to the experimentally observed ones. However, simulated curves show precursor events which are not reflected in the data. Models proposed by CNSC and LBNL are the only approaches capable of reasonably capturing the exact timing when breakthrough occurs, see Table 8.

Table 8 Capabilities of the proposed models regarding stress evolution (✓: good, ~: fair; blank: poor; -: results not provided or not applicable).

Model	Stress														
	Peak value					Post-peak shape					Timing				
	1	2	3	I	B	1	2	3	I	B	1	2	3	I	B
BGR/UFZ	✓	✓	✓	-	~	✓	✓	✓	-	✓		✓	✓	-	✓
CNSC-E											✓	~	~	✓	✓
CNSC-D	✓			~		✓			✓		✓	~	~	~	~
KAERI				✓	~	✓	✓	✓	✓	✓					
LBNL-C	✓	✓	✓	✓	✓						✓	✓	✓	✓	✓
LBNL-D	~	~	✓	✓	~	✓	✓	✓	✓	✓	✓	✓	✓	✓	✓
NCU/TPC															
Quintessa/RWM	✓	✓	✓	✓	✓									~	
UPC/Andra-H															
UPC/Andra-HM1			~	✓		✓	✓	✓	✓	✓		~	✓		~
UPC/Andra-HM2	~			✓		✓	✓	✓	✓	✓					

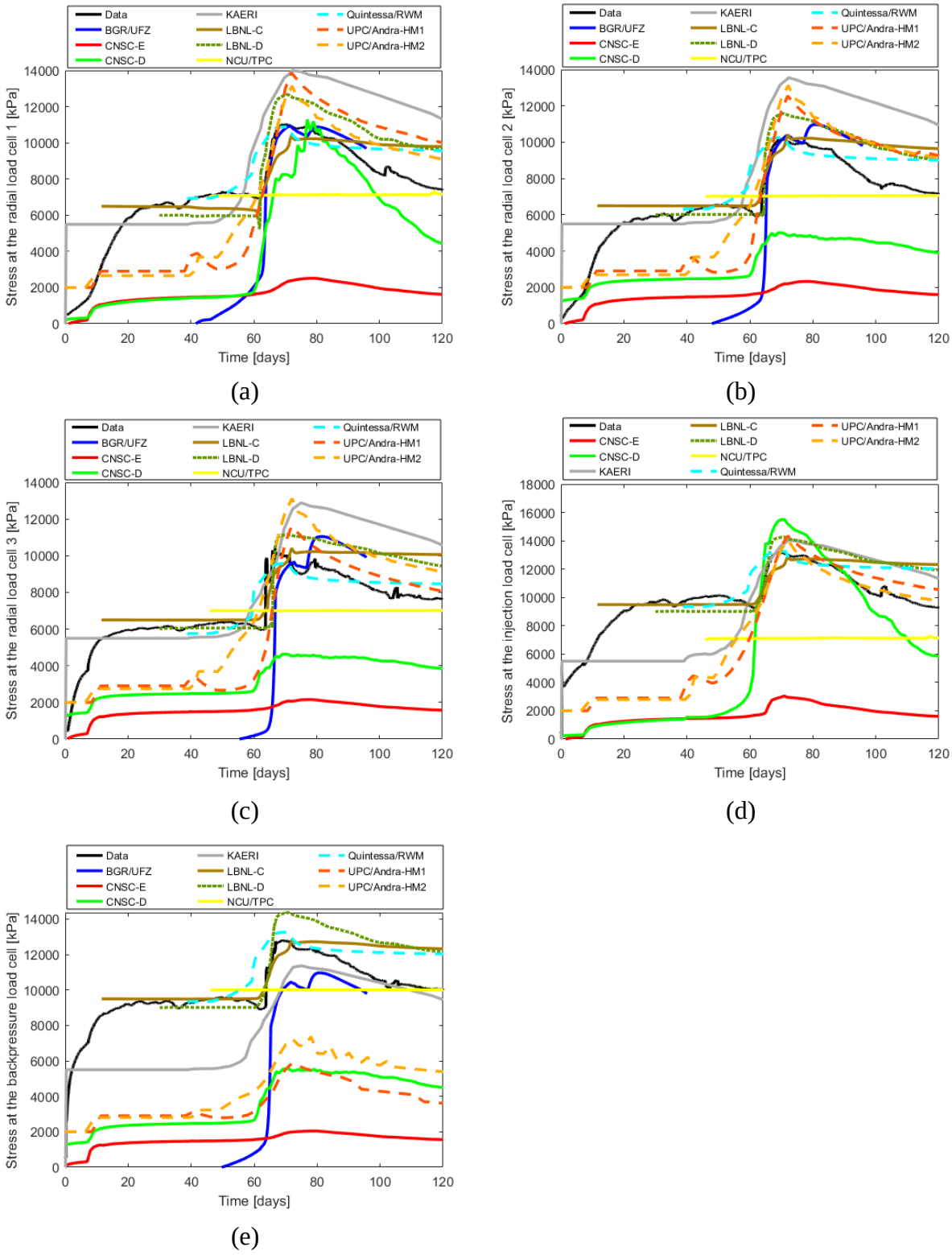

Figure 10 Comparison of modelled versus observed stress evolution at (a) radial load cell 1, (b) radial load cell 2, (c) radial load cell 3, (d) injection load cell and (e) backpressure load cell.

Pore pressure evolutions at three different locations (arrays 1, 2 and 3) are shown in Figure 11. It is important to note that before gas breakthrough, pore pressure equals porewater pressure. However, once gas enters the filter, this is actually measuring local gas pressure. As seen, models KAERI, LBNL-D and UPC/Andra-HM2 are able to properly capture the peak value at all the arrays. The continuous model proposed by LBNL provides good predicted peak values in sensors 1 and 2 but the breakthrough pore pressure at sensor 3 is slightly overpredicted. Reasonably good peak values are also obtained with BGR/UFZ and UPC/Andra-HM1 models. However, at these arrays, highly overpredicted (with model UPC/Andra-H) and underpredicted (CNSC-E, CNSC-D, Quintessa/RWM) values are also obtained. As happened with the stress response, (i) the post-peak shape trend is well defined by almost all models and only Quintessa/RWM and CNSC-E fail in describing the post-peak curve (now model LBNL-C provides good post-peak shape fitting) and (ii) the two models proposed by CNSC and LBNL are the only approaches capable of properly capturing the timing when breakthrough occurs, see Table 9. As happened also with the stress response, the rapid increase in pore pressure is modelled by many of the teams. However, this is obtained at early times by some of them.

Table 9 Capabilities of the proposed models regarding pore pressure evolution (✓: good, ~: fair; blank: poor).

Model	Pore pressure								
	Peak value			Post-peak shape			Timing		
	1	2	3	1	2	3	1	2	3
BGR/UFZ	✓	~	~	✓	✓	✓			✓
CNSC-E							✓	✓	✓
CNSC-D				✓	✓	✓	~	~	~
KAERI	✓	✓	✓	✓	✓	✓			✓
LBNL-C	✓	✓	~	✓	✓	✓	✓	✓	✓
LBNL-D	✓	✓	✓	✓	✓	✓	✓	✓	✓
NCU/TPC									
Quintessa/RWM									~
UPC/Andra-H				✓	✓	✓			
UPC/Andra-HM1	~	~	~	✓	✓	✓	~	~	~
UPC/Andra-HM2	✓	✓	✓	✓	✓	✓			

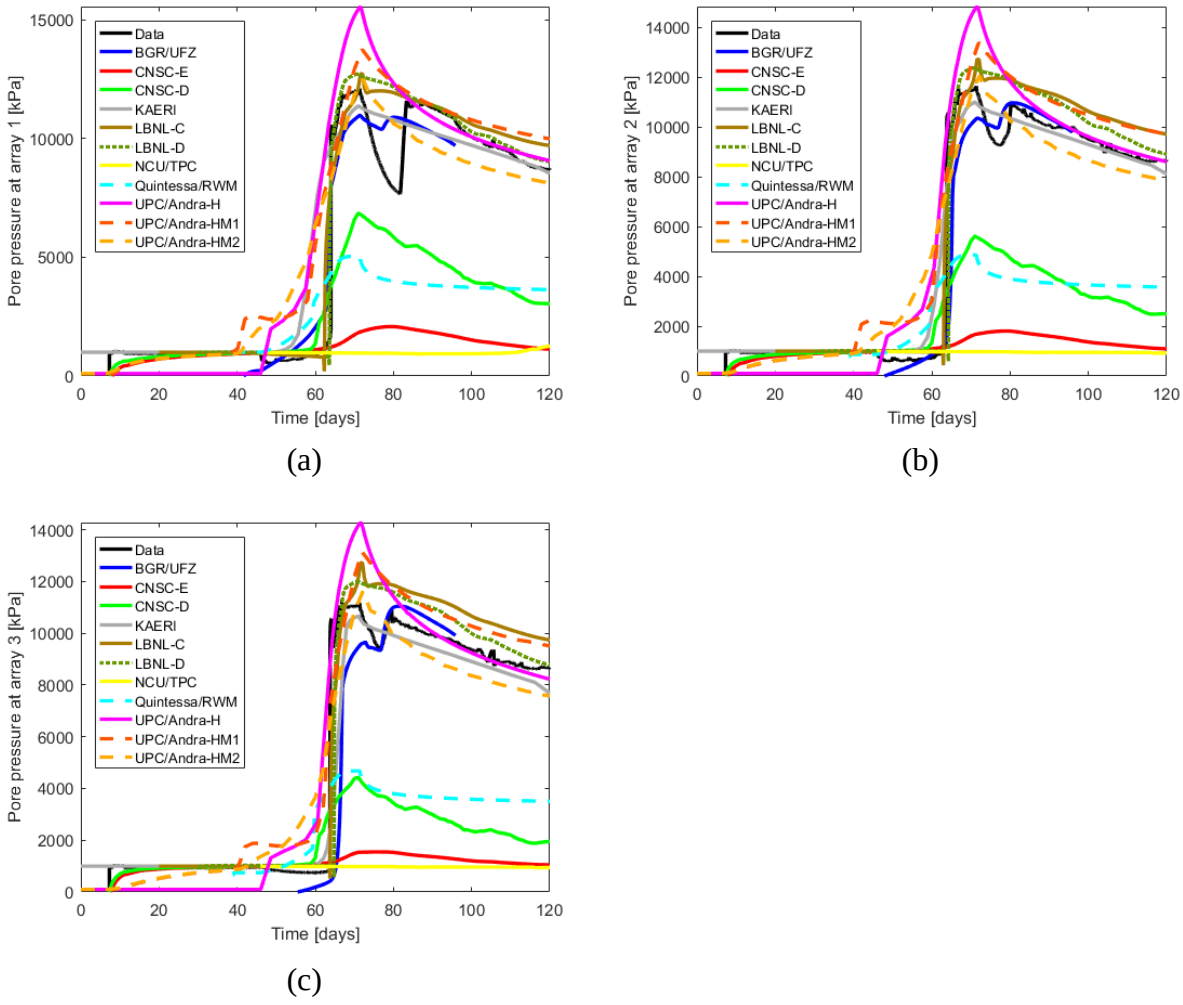

Figure 11 Comparison of modelled versus observed pore pressures at array (a) 1, (b) 2 and (c) 3.

5 Conclusions

The different modelling teams have shown that a wide range of models may be applied to numerically describe gas migration in plastic clays, see Table 10. At this stage of the modelling exercise, models have been validated against a single experiment and thus, future work is still needed to further develop them. So far, existing fits show that after a calibration process (often a very large set of input parameters need to be adjusted), plausible descriptions of the laboratory experiment can be achieved. In a number of cases, these realizations required adjustment of porosity and intrinsic permeability values beyond specified parameters for the material, suggesting the physical description of the system remains incomplete.

Two-phase flow models (with different deformation behaviours and/or preferential pathways) have been implemented to model gas flow. These approaches are able to match some key aspects such as stress evolution or pore pressure but they are not capable of describing the full complexity of gas migration processes in such low-permeability materials. Thus, although they are highly extended and employed, the modelling to date suggests that two-phase flow models are not capable of reproducing the full range of behaviour exhibited experimentally, so their practicality will

depend upon the intended usage. Discrete approaches to describe dilatancy-controlled gas flow have shown physically plausible representations can be obtained noting that extra effort is required to calibrate such a large set (even larger) of input parameters. New conceptual models may be hence developed to explain the complexity of the physical processes. Their development is still in a very preliminary phase and at the current stage of the work, they are not able to reproduce physically-observed features. Thus, from a pragmatic perspective, enhanced two-phase flow models (either by different deformation behaviours, explicitly incorporating different pathways and/or evolving fractures) remain the only viable tool to represent these systems at this time. However, the complexity of the physical processes combined with detailed calibration processes, currently limit their use in the quantitative prediction of gas flow.

Table 10 Summary of the proposed strategies.

Model	Approach	Software	Basic parameters				Results																										
							Flow		Stress																		Pore pressure								
									P					S					T						P			S			T		
			E	ν	ϕ	k	P	S	1	2	3	I	B	1	2	3	I	B	1	2	3	I	B	1	2	3	1	2	3	1	2	3	1	2	3
BGR/UFZ	2D 2-phase flow	OpenGeoSys	✓	✓	✓		✓		✓	✓	✓	-	~	✓	✓	✓	-	✓		✓	✓	-	✓	✓	~	~	✓	✓	✓			✓			
CNSC-E	3D 2-phase flow	COMSOL®	✓	✓	✓	✓													✓	~	~	✓	✓							✓	✓	✓		
CNSC-D	3D 2-phase flow	COMSOL®	✓	✓	✓	✓			✓			~		✓			✓		✓	~	~	~	~				✓	✓	✓	~	~	~		
KAERI	3D 2-phase flow	TOUGH-MP FLAC3D	✓	✓	✓	✓		✓				✓	~	✓	✓	✓	✓	✓						✓	✓	✓	✓	✓	✓			✓		
LBNL-C	3D 2-phase flow	TOUGH-FLAC	✓	✓	✓	✓	✓		✓	✓	✓	✓	✓						✓	✓	✓	✓	✓	✓	✓	~	✓	✓	✓	✓	✓	✓		
LBNL-D	2D discrete	TOUGH-RBSN	✓	✓	✓	✓	✓		~	~	✓	✓	~	✓	✓	✓	✓	✓	✓	✓	✓	✓	✓	✓	✓	✓	✓	✓	✓	✓	✓	✓	✓	✓
NCU/TPC	2D 2-phase flow	THMC 7.1	✓	✓			-	-																									
Quintessa/RWM	1D 2-phase flow + pathways	QPAC	✓	✓	-	✓	✓		✓	✓	✓	✓	✓									~												~
Sandia	discrete		-	-	-	-	-	-	-	-	-	-	-	-	-	-	-	-	-	-	-	-	-	-	-	-	-	-	-	-	-	-	-	-
UPC/Andra-H	3D 2-phase flow	CODE_BRIGHT	-	-					-	-	-	-	-	-	-	-	-	-	-	-	-	-	-				✓	✓	✓					
UPC/Andra-HM1	3D 2-phase flow + pathways	CODE_BRIGHT									~	✓		✓	✓	✓	✓	✓		~	✓		~	~	~	~	✓	✓	✓	~	~	~		
UPC/Andra-HM2	3D 2-phase flow + pathways	CODE_BRIGHT	✓	✓					~			✓		✓	✓	✓	✓	✓						✓	✓	✓	✓	✓	✓					

6 Planned and completed publications

Table 11 Planned and completed journal and conference papers (peer-reviewed publications) for Task A.

Author(s)	Title	Journal/Conference	Status
Tamayo-Mas, E., Harrington, J.F, Shao, H., Dagher, E.E., Lee, J., Kim, K., Rutqvist, J., Lai, S.H., Chittenden, N., Wang, Y., Damians, I.P. and Olivella, S.	Numerical modelling of gas flow in a compact clay barrier for DECOVALEX-2019	Second International Discrete Fracture Network Engineering Conference	Provisionally accepted

Table 12 Other planned and completed contributions (conference talks, posters...) for Task A.

Author(s)	Title	Journal / Conference	Type of publication	Status

References

British Geological Survey holds most of the references listed below, and copies may be obtained via the library service subject to copyright legislation (contact libuser@bgs.ac.uk for details). The library catalogue is available at: https://envirolib.apps.nerc.ac.uk/olibcgi.

Angeli, M., M. Soldal, E. Skurtveit and E. Aker. (2009). Experimental percolation of supercritical CO2 through a caprock. *Energy Procedia*. 1, 3351-3358. doi: 10.1016/j.egypro.2009.02.123.

Asahina, D., J.E. Houseworth, J.T. Birkholzer, J. Rutqvist and J.E. Bolander. (2014). Hydro-mechanical model for wetting/drying and fracture development in geomaterials. *Computers and Geosciences.* 65, 13-23. doi: 10.1016/j.cageo.2013.12.009.

Bani-Yaghoub, M. (2017). Analysis and applications of delay differential equations in biology and medicine, arXiv:1701.04173v1.

Bandis, S.C., A.C. Lumsden and N.R. Barton. (1983). Fundamentals of rock joint deformation. *International Journal of Rock Mechanics and Mining Sciences and Geomechanic Abstracts.* 20, 249–68. doi: 10.1016/0148-9062(83)90595-8.

COMSOL. 2017. COMSOL Multiphysics version 5.3a. Manual.

Daniels, K.A. and J.F. Harrington. (2017). The Response of Compact Bentonite during a 1D Gas Flow Test. *British Geological Survey Open Report*, OR/17/067. 19pp.

Fall, M., O. Nasir and T.S. Nguyen. (2014). A coupled hydro-mechanical model for simulation of gas migration in host sedimentary rocks for nuclear waste repositories. *Engineering Geology*. 176, 24-44. doi: 10.1016/j.enggeo.2014.04.003.

Harrington, J.F. and S.T. Horseman. (1999). Gas transport properties of clays and mudrocks. In Muds and Mudstones: Physical and Fluid Flow Properties, ed. A.C. Aplin, A.J. Fleet and J.H.S. Macquaker. *Geological Society of London Special Publications.* 158. Geological Society of London, London, 107-124. doi: 10.1144/GSL.SP.1999.158.01.09.

Harrington, J.F. and S.T. Horseman. (2003). Gas migration in KBS-3 buffer bentonite: Sensitivity of test parameters to experimental boundary conditions. *Report TR-03-02*. Svensk Kärbränslehantering AB (SKB), Stockholm, Sweden.

Harrington, J.F., C.C. Graham, R.J. Cuss and S. Norris. (2017a). Gas network development in a precompacted bentonite experiment: Evidence of generation and evolution. *Applied Clay Science*. 147, 80-89. doi: 10.1016/j.clay.2017.07.005.

Harrington, J.F., R.J. Cuss and J. Talandier. (2017b). Gas transport properties through intact and fractured Callovo-Oxfordian mudstones. In Rutter, E. H., Mecklenburgh, J. & Taylor, K. G. (eds) Geomechanical and Petrophysical Properties of Mudrocks. *Geological Society of London Special Publications*. 454. doi: 10.1144/SP454.7.

Horseman, S.T., J.F. Harrington and P. Sellin. (1996). Gas migration in Mx80 buffer bentonite. *Materials Research Society Proceedings.* 465, 1003-1010. doi: 10.1557/PROC-465-1003.

Horseman, S.T., J.F. Harrington and P. Sellin. (2004). Water and gas flow in Mx80 bentonite buffer clay. *Materials Research Society Proceedings.* 807, 715-720. doi: 10.1557/PROC-807-715.

Itasca, FLAC3D Version 6.0. (2018). Fast Lagrangian Analysis of Continua in 3 Dimensions. ITASCA Consulting Group Inc. https://www.itascacg.com/software/flac3d

Kawai, T. (1978). New discrete models and their application to seismic response analysis of structures. *Nuclear Engineering and Design.* 48, 207-229. doi: 10.1016/0029-5493(78)90217-0.

Khalili, N. and M.H. Khabbaz. (1998). A unique relationship for χ for the determination of the shear strength of unsaturated soils. *Géotechnique.* 48, 1-7. doi: 10.1680/geot.1998.48.5.681.

Kolditz, O., S. Bauer, L. Bilke, N. Böttcher, J.O. Delfs, T. Fischer, U.J. Görke, T. Kalbacher, G. Kosakowski, C.I. McDermott, C.H. Park, F. Radu, K. Rink, H. Shao, H.B. Shao, F. Sun, Y.Y. Sun, A.K. Singh, J. Taron, M. Walther, W. Wang, N. Watanabe, N. Wu, M. Xie, W. Xu and B. Zehner. (2012). OpenGeoSys: An open-source initiative for numerical simulation of thermo-hydro-mechanical/chemical (THM/C) processes in porous media. *Environmental Earth Sciences*. 67, 589-599. doi: 10.1007/s12665-012-1546-x.

Marschall P., S.T. Horseman and T. Gimmi. (2005). Characterisation of gas transport properties of the Opalinus Clay, a potential host rock formation for radioactive waste disposal. *Oil & Gas Science and Technology – Revue de l'Institute Frances Petrole.* 60, 121–139. doi: 10.2516/ogst:2005008.

Nasir, O., T.S. Nguyen, J.D. Barnichon and A. Millard. (2016). Simulation of hydromechanical behaviour of bentonite seals for containment of radioactive wastes. *Canadian Geotechnical Journal*. 54, 1055-1070. doi: 10.1139/cgj-2016-0102.

Olivella, S., A. Gens, J. Carrera and E.E. Alonso. (1996). Numerical formulation for a simulator (CODE_BRIGHT) for the coupled analysis of saline media. *Engineering Computations.* 13, 87-112. doi: 10.1108/02644409610151575.

Olivella, S. and E.E. Alonso. (2008). Gas flow through clay barriers. *Géotechnique.* 58, 157-176. doi: 10.1680/geot.2008.58.3.157.

Ortiz, L., G. Volckaert and D. Mallants. (2002). Gas generation and migration in Boom Clay, a potential host rock formation for nuclear waste storage. *Engineering Geology.* 64, 287-296. doi: 10.1016/S0013-7952(01)00107-7.

Quintessa. (2013). QPAC: Quintessa's General-Purpose Modelling Software QRS-QPAC-11. http://www.quintessa.org/qpac-overview-report.pdf

Rodwell, W.R., A.W. Harris, S.T. Horseman, P. Lalieux, W. Müller, L. Ortiz Amaya and K. Pruess. (1999). Gas Migration and Two-Phase Flow through Engineered and Geological Barriers for a Deep Repository for Radioactive Waste. *European Commission*, Report EUR19122EN.

Rutqvist, J. (2011). Status of the TOUGH-FLAC simulator and recent applications related to coupled fluid flow and crustal deformations. *Computers and Geosciences.* 37, 739-750. doi: 10.1016/j.cageo.2010.08.006.

Strogatz, S.H. (2001). Nonlinear Dynamics and Chaos: With Applications to Physics, Biology, Chemistry, and Engineering, *Westview*.

van Genuchten, M.T. (1980). A closed-form equation for predicting the hydraulic conductivity of unsaturated soils. *Soil science society of America journal.* 44, 892-898. doi: 10.2136/sssaj1980.03615995004400050002x.

Weetjens, E. and X. Sillen. (2006). Gas Generation and Migration in the Near Field of a Supercontainer-Based Disposal System for Vitrified High-Level Radioactive Waste. In *Proceedings of the 11th International High-Level Radioactive Waste Management Conf. (IHLRWM)*, Las Vegas, Nevada, USA, April 30 – May 4.

Wikramaratna, R.S., M. Goodfield, W.R. Rodwell, P.J. Nash and P.J. Agg. (1993). A Preliminary Assessment of Gas Migration from the Copper/Steel Canister. *Report TR-93-31*. Svensk Kärbränslehantering AB (SKB), Stockholm, Sweden.

Xu, W.J., H. Shao, J. Hesser, W. Wang, K. Schuster and O. Kolditz. (2013). Coupled multiphase flow and elasto-plastic modelling of in-situ gas injection experiments in saturated claystone (Mont Terri Rock Laboratory). *Engineering Geology.* 157, 55-68. doi: 10.1016/j.enggeo.2013.02.005.

Yeh, G.T., C.H. Tsai and I.S. Liu. (2013). GMech: A Geo-Mechanics Model for Finite Visco-Elastic Materials: Theoretcal Basis and Numerical Approximation. *Graduate Institute of Applied Geology*, National Central University, Jhongli City, Taoyuan County, Taiwan.

Zhang, K. Y.S. Wu and K. Pruess. (2008). User's guide for TOUGH2-MP- A massively parallel version of the TOUGH2 code. Earth Sciences Division, Lawrence Berkeley National Laboratory. https://escholarship.org/uc/item/00d9040f.